


Article

Application of AIRS Soundings to Afternoon Convection Forecasting and Nowcasting at Airports

Nan-Ching Yeh¹, Yao-Chung Chuang^{2,*}, Hsin-Shuo Peng³ and Chih-Ying Chen⁴ 

¹ Department of Military Meteorology, Air Force Institute of Technology, Kaohsiung 82047, Taiwan; Trea024@afats.khc.edu.tw

² Department of Aviation & Communication Electronics, Air Force Institute of Technology, Kaohsiung 82047, Taiwan

³ Naval Meteorological and Oceanographic Office, Kaohsiung 81300, Taiwan; qqmoaso@gmail.com

⁴ Research Center for Environmental Changes, Academia Sinica, Taipei 11529, Taiwan; cycch6914@gate.sinica.edu.tw

* Correspondence: physicsmoon1213@gmail.com or Tree063@afats.khc.edu.tw

Abstract: In Taiwan, the frequency of afternoon convection increases in summer (July and August), and the peak hour of afternoon convection occurs at 1500–1600 local solar time (LST). Afternoon convection events are forecasted based on the atmospheric stability index, as computed from the 0800 LST radiosonde data. However, the temporal and spatial resolution and forecast precision are not satisfactory. This study used the observation data of Aqua satellite overpass near Taiwan around 1–3 h before the occurrence of afternoon convection. Its advantages are that it improves the prediction accuracy and increases the data coverage area, which means that more airports can use results of this research, especially those without radiosondes. In order to determine the availability of Atmospheric Infrared Sounder (AIRS) in Taiwan, 2010–2016 AIRS and radiosonde-sounding data were used to determine the accuracy of AIRS. This study also used 2017–2018 AIRS data to establish K index (KI) and total precipitable water (TPW) thresholds for the occurrence of afternoon convection of four airports in Taiwan. Finally, the KI and TPW were calculated using the independent AIRS atmospheric sounding (2019–2020) to forecast the occurrence of afternoon convection at each airport. The average predictive accuracy rate of the four airports is 84%. Case studies at Hualien Airport show the average predictive accuracy rate of this study is 81.8%, which is 9.1% higher than that of the traditional sounding forecast (72.7%) during the same period. Research results show that using AIRS data to predict afternoon convection in this study could not only increase data coverage area but also improve the accuracy of the prediction effectively.

Keywords: afternoon convection; atmospheric stability index; radiosonde; AIRS; K index; total precipitable water



Citation: Yeh, N.-C.; Chuang, Y.-C.; Peng, H.-S.; Chen, C.-Y. Application of AIRS Soundings to Afternoon Convection Forecasting and Nowcasting at Airports. *Atmosphere* **2022**, *13*, 61. <https://doi.org/10.3390/atmos13010061>

Academic Editors: Zuohao Cao, Huaqing Cai and Xiaofan Li

Received: 19 November 2021

Accepted: 28 December 2021

Published: 30 December 2021

Publisher's Note: MDPI stays neutral with regard to jurisdictional claims in published maps and institutional affiliations.



Copyright: © 2021 by the authors. Licensee MDPI, Basel, Switzerland. This article is an open access article distributed under the terms and conditions of the Creative Commons Attribution (CC BY) license (<https://creativecommons.org/licenses/by/4.0/>).

1. Introduction

Heavy convection storms are relevant to flight safety during takeoff and landing. The World Meteorological Organization (WMO) defined nowcasting as forecasting with local detail, by any method, over a period from the present to six hours ahead, including a detailed description of the present weather. It is thus of great concern to aeronautical meteorological forecasting and nowcasting. When deep convection occurs in Taiwan, the temperature and humidity of each vertical layer of the atmospheric environment increase [1,2]. Relative to typhoons and the Meiyu front, the afternoon convection system exhibits a smaller spatial scale and shorter lifetime, so it is very difficult to predict the start time, initial location, and duration of afternoon convection [1,3,4]. Even if the rainfall pattern has great variability, it is very important to estimate the rainfall characteristics of different scales, seasons, and environments [5–8].

Radiosonde measurements of the atmospheric stability index can be used to predict severe weather development; such measurements are considered to be a representative of the synoptic scale environment [9]. Researchers have compared various atmospheric stability indices calculated from radiosonde observations to analyze the correlation between the stability index and cumulative precipitable water and have found the K index (KI) to be the most suitable index for forecasting heavy rain events [10,11]. Using numerical models to simulate rainfall studies, the KI can provide useful forecast guidance for rainfall events [12].

When a weather balloon is launched from the ground to the stratosphere, the balloon is horizontally displaced by tens of kilometers due to the wind field of the height [13]. Weather balloons are launched daily to record local vertical atmospheric parameters in the vicinity of where the balloon was launched. Taking the main island of Taiwan as an example, only two of the radiosonde observations of the Central Weather Bureau (CWB) can be obtained online. Thus, in Taiwan, the spatial distribution of weather balloons is insufficiently broad. The use of satellites, given their wide observational swath, compensates for these spatial distribution-related shortcomings in sounding.

Atmospheric stability index on pre-convective atmospheric stability and changes in boundary-layer structure are crucial [14]. Forecasters obtain data on atmospheric stability from the weather balloons launched at 00 UTC (i.e., 08am LST). They use such data as a basis for forecasting afternoon convection because atmospheric stability relates to the development of afternoon convection. The problem is the launch time of the weather balloons differs by 7–8 h from the afternoon convection's extremum (1500–1600 LST), and atmospheric-environmental changes during this period can result in forecasting error. Therefore, the use of weather balloons is inadequate because of limitations in data volume, coverage area, and immediacy.

As a remedy, Aqua satellite can be used. This satellite, which has an Atmospheric Infrared Sounder (AIRS) mounted on it, passes Taiwan 1–3 h before the extremum of afternoon convection. Numerous studies have shown that AIRS can provide a three-dimensional field with respect to variation characteristics of temperature, specific humidity, etc. [15–19]. Specifically, the AIRS observes the atmospheric environment at a time that is closer to the time at which afternoon convection occurs. Thus, relative to the use of radiosonde observation data, the use of Aqua satellite yields more accurate forecasts. However, there is a limitation in the use of polar-orbiting satellite Aqua. The satellites orbits and swaths will be shifted a bit, and there is no data to use outside of the swath. Total precipitable water (TPW) is the total amount of precipitable water in an atmospheric column between the Earth's surface and space. Regardless of the phases, its value, variability, and trends have a great influence on rainfall events [20–24].

The main objective of this study is to use satellite data to establish an atmospheric stability index and TPW threshold. These indicators can be used by forecasters to better predict the summer occurrence of afternoon convection in various airports in Taiwan, thus allowing them to anticipate possible weather changes.

2. Materials and Methods

2.1. Data

The data used in this study include Aqua satellite data, ground observation data, and radiosonde data. The data period is July and August from 2010 to 2020. Its purpose includes testing the reliability of satellite data, systematic error analysis and correction, the establishment of rainfall thresholds, and case verification. The details of the above data are as shown in Section 2.2.1, Section 2.2.2, Section 2.2.3.

2.1.1. AIRS

NASA's Aqua Satellite is part of the A-Train constellation of orbiting satellites. The satellite is equipped with six different earth observation systems, being able to obtain data on various parameters relating to the land, ocean, atmosphere, and biosphere [25]. AIRS has a scanning width of 2330 km, a nadir point horizontal resolution of 13.5 km, and can

gather data on the entire planet in 2 days. AIRS comprises a hyperspectral sounder with 2378 infrared channels as well as four visible-light and near-infrared channels, allowing it to measure infrared radiation from the earth's surface and atmosphere [26,27]. Moreover, AIRS can measure various parameters pertaining to the physical properties of clouds and the thermodynamics of the atmosphere. In addition to weather monitoring, AIRS can also be applied to data model assimilation and the study of the climate [28–30].

AIRS can undertake high-precision atmospheric sounding due to its multiple channels under clear and partly cloudy conditions [15], but lower-tropospheric measurements are susceptible to sea conditions [31]. These differences significantly affect measurements of the stable structure of the low troposphere. In response, numerous studies have devised various methods for modifying AIRS-measured data [32–34]. This study used the AIRS Level 2 dataset (AIRX2RET) in July and August 2010–2020. The dataset provided daily global temperature and moisture profiles with an accuracy of 1 K per 1-km-thick and of 15% per 2-km-thick in the troposphere [35].

2.1.2. Atmospheric Sounding

Since 1958, the radiosonde has been the only instrument used for the long-term observation of temperature distributions in the troposphere to low stratosphere [36]. The radiosonde is often used as reference data in gauging the validity of water vapor obtained from other techniques [37–39]. Globally distributed sounding stations provide in situ radiosonde observations for assessing the state of the vertical atmosphere [31]. The weather balloon is launched from the ground to the stratosphere with an average horizontal displacement of about 50 km [13]. Therefore, the radiosonde observation represents the atmospheric conditions within a radius of 50 km from the balloon launch location. However, the temporal and spatial resolution of radiosondes is inadequate for use in forecasting.

This study used radiosonde data on Hualien and Banqiao from the CWB of Taiwan; the radiosonde locations are marked by a black star in Figure 1. In general, radiosonde data have errors from encoding, data transmission, and decoding. In this study, the method proposed by Chen (1994) [40] was used to verify the radiosonde data's accuracy.

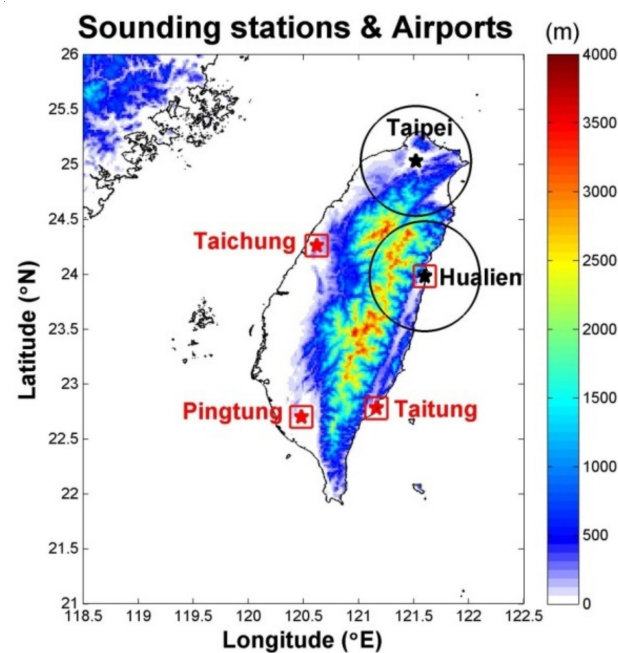


Figure 1. Highly distributed terrain in Taiwan; black stars represent sounding stations and red squares represent airport locations.

The uncertainty of temperature and relative humidity at upper-air network data observed by Vaisala RS-92 radiosonde was below 1 °C and 6% respectively [41]. Moreover,

different brands of radiosondes have different observation errors in different seasons, regions, and even day and night [36,42–44]. Therefore, only 00-UTC radiosonde data required for practical applications were used for the conduct of its comparison of atmospheric sounding data. The models for both sets of data were Vaisala radiosonde models, which feature more consistent uncertainties. This study used atmospheric sounding data for the same time period as AIRS. Table 1 presents the radiosonde information used in this study.

Table 1. Information related to the radiosonde observations used to evaluate the AIRS thermodynamic profiles.

Site Name	Location	Launch Frequency (Per Day)	No. of Profiles (Day Time Only)	Time Period for Evaluation	Radiosonde Manufacturer/Model
Taipei	25.03° N 121.52° E	2	229	July–August from 2010–2016	Vaisala RS-92/RS-41
Hualien	23.98° N 121.6° E	2	219		

2.1.3. Surface Observations

The Meteorological Terminal Aviation Routine Weather Report (METAR) is a format for reporting aeronautical meteorological observations. A special (SPECI) report is drafted if weather conditions change significantly during the two METAR observation intervals. The METAR/SPECI observations include cloud coverage, phenomenon (e.g., rainfall), and cumulative rainfall. The above parameters are used in this study.

This study predicted the occurrence of convection in the weak synoptic scale for the airports in July and August. The determination of “weak weather scale” and “occurring convection” is based on the observation data of METAR/SPECI.

2.2. Methodology

This study used July and August 2010–2016 data from the Banqiao and Hualien radiosonde stations. Problematic data were deleted [40] and compared with data from within the AIRS’ swath and from the radiosonde stations. The systematic errors in the AIRS data for Taiwan were analyzed and corrected according to the linear regression equations for each altitude, which were in terms of the temperature and dew point. Subsequently, the corresponding atmospheric stability index was calculated based on corrected and reliable temperature and dew point.

Finally, in conjunction with AIRS-retrieved TPW, the thresholds of afternoon convection at each airport were established and verified with independent data. More specifically, July and August 2017–2018 data were used for obtaining the threshold for afternoon convective rainfall; therefore, the accuracy of predicting afternoon convection used independent data from 2019–2020.

2.2.1. Validation of AIRS Temperature and Dew Point Profiles

Although the temperature and water vapor accuracy of AIRS in the troposphere are 1 K and 15%, respectively [35]. However, the uncertainty of sounding measurements varies with region [36,44], and the difference in temperature and humidity between AIRS and radiosondes in the low troposphere varies with seasons [31]. Therefore, soundings must be compared before use to ensure the correctness of the AIRS’ measurements of temperature and humidity. In addition, this study focused only on afternoon convection in Taiwan and thus only analyzed the months (July and August) when afternoon convection most frequently occurs.

In this study, radiosonde data were used to validate AIRS’ atmospheric sounding measurements. July and August 2010–2016 data were compared, and July and August 2017–2018 data were used for verifying the credibility of temperature and dew point of AIRS. Research has revealed differences between the deviations of day and night radiosonde observations [36,43]. Therefore, only 00 UTC data is used for comparison, correction, and verification between AIRS and radiosonde observations.

For reasons such as AIRS’s swath not providing coverage up to the sounding station and sounding data failing the quality inspection procedure [40], the number of comparison samples was fewer than the number of soundings administered. In this study, because the temperature and humidity of 850, 700, and 500 hPa were used to calculate KI, the temperatures and humidity of these three levels were compared. The observations can be regarded as representative of atmospheric conditions within a 50-km radius [13]. Therefore, a radiosonde station was used as the center, where the average of all AIRS field of View (FOV) within a 50-km radius was used as the AIRS-retrieved measurements (as marked by the black circles in Figure 1).

2.2.2. Confirmation and Correction of Systemic Errors

Figure 2 presents the temperature and dew point scatter plot for AIRS and radiosonde measurements. The abscissa represents AIRS measurements, and the ordinate represents radiosonde measurements. Figure 2a illustrates the temperature distribution for 850, 700, and 500 hPa, and Figure 2b illustrates the dew point distribution for 850, 700, and 500 hPa. The blue dotted line represents the fitted straight-line equation, and the green solid line represents the reference equation $x = y$. Tables 2 and 3 present the correlation coefficients, temperature, and dew point fitting equations for each level.

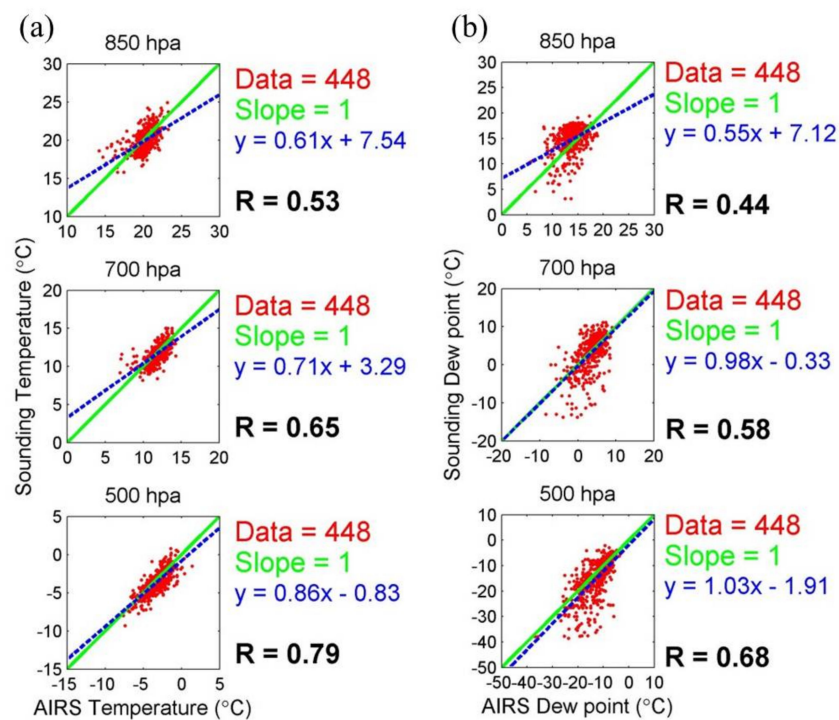


Figure 2. AIRS and sounding scatter plots of 850, 700, 500 hPa from top to bottom for (a) temperature and (b) dew point.

Table 2. Temperature correlation coefficients and linear regression equations for each level of 00Z for July and August of 2010–2016.

High-Altitude Level	Number of Data	Correlation Coefficient	Regression Equation
500 hPa	448	0.79	$y = 0.86x - 0.83$
700 hPa	448	0.65	$y = 0.71x + 3.29$
850 hPa	448	0.53	$y = 0.61x + 7.54$

Table 3. Dew point correlation coefficients and linear regression equations for each level of 00Z for July and August of 2010–2016.

High-Altitude Level	Number of Data	Correlation Coefficient	Regression Equation
500 hPa	448	0.68	$y = 1.03x - 1.91$
700 hPa	448	0.58	$y = 0.98x - 0.33$
850 hPa	448	0.44	$y = 0.55x + 7.12$

As evident in Figure 2, the temperature distribution is more concentrated than the dew point distribution. In other words, the change in temperature was less obvious than the change in dew point, consistent with the results of Ingleby (2017) [44], where dew point uncertainty was greater than that for temperature. Data spanning 7 years were used to establish the modified equations, and 2 years of independent data for each level were included in the corresponding modified equation. In doing these, the temperature and dew point data more accurately represented the actual atmospheric environment.

2.2.3. Forecast Rules and Probability Using K Index and Total Precipitable Water

This study identified KI to be the most suitable index from different stability indices for forecasting afternoon convection in Taiwan. There are similar results in several different areas [10–12]. KI is considered to have the static stability of the 850–500-mb layer, and the mathematical formula for KI is as follows [45].

$$KI = (T_{850} - T_{500}) + Td_{850} - (T_{700} - Td_{700}) \quad (1)$$

T_{850} , T_{700} , and T_{500} are the temperatures at 850, 700, and 500 hPa, respectively, and Td_{850} and Td_{700} are the dew points at 850 and 700 hPa, respectively. KI includes the factors of a lapse rate of temperature of 850–500 hPa, a dew point of 850 hPa, and a saturation level of 700 hPa; the sum of all three factors represents the potential of a thunderstorm and rainfall. KI is higher, and the chance of thunderstorms/rainfall is higher.

The middle-troposphere humidity is a vital factor explaining the occurrence and development of convection [46]. KI includes the 850–500 hPa lapse rate of temperature and the water vapor content in the middle and low troposphere [12]. Therefore, KI can be used as a reference for predicting afternoon convection. In addition to KI, TPW is an essential indicator [21,23,24]. When TPW is low, convection will not occur even if the atmospheric environment is unstable.

The afternoon convection threshold must be evaluated separately for each airport, because the threshold of thunderstorm occurrence changes depending on location [47]. The evaluation of predictive accuracy is illustrated in Figure 3; the abscissa is TPW, the ordinate is KI, and the red dotted lines are the thresholds of KI and TPW (hereafter abbreviated as K_h and T_h , respectively). Both dotted lines divide the atmospheric-environmental parameters into four quadrants, named quadrants 1 to 4 (Q1–Q4).

Q1 represents when $TPW > T_h$ and when the atmosphere is unstable (i.e., $KI > K_h$), entailing a forecast that convection will occur in the afternoon. By contrast, Q3 represents when $TPW < T_h$ and when the atmosphere is stable (i.e., $KI < K_h$), entailing a forecast that convection will not occur in the afternoon. Furthermore, Q2 ($KI > K_h$ and $TPW < T_h$) and Q4 ($KI < K_h$ and $TPW > T_h$) entail a forecast that precipitation will not occur.

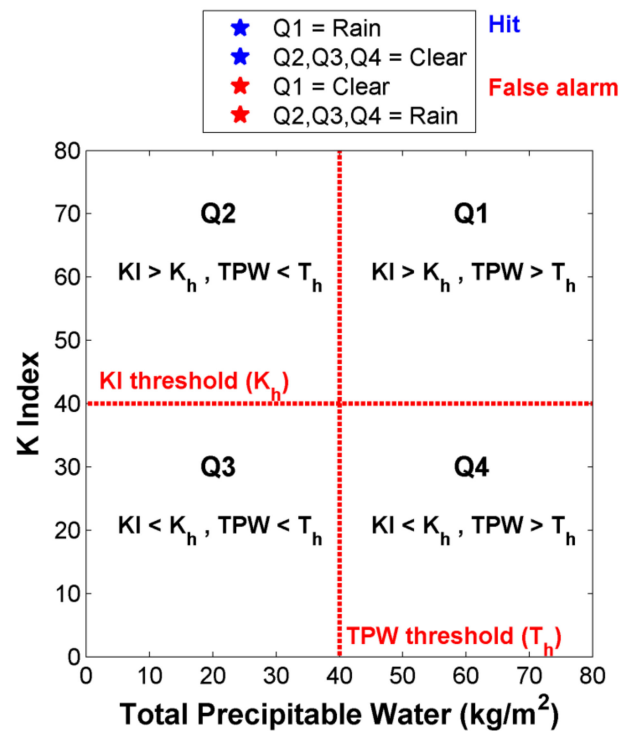


Figure 3. Evaluation of accuracy for TPW and KI of the afternoon convection of each airport.

3. Results and Discussion

3.1. AIRS Comparison Results

The comparison of temperature and dew point used 2010–2016 data, and 2017–2018 data were used to verify its accuracy. The 2019–2020 data is used to estimate how much the forecast results of this study have improved. The comparison between measurements obtained from AIRS atmospheric sounding and that obtained from radiosonde observations is illustrated in Figure 4. Figure 4a,b illustrate, for each level, the comparison between temperature and dew point, respectively. The blue line represents the AIRS retrieval value, and the red line represents the radiosonde observations (sample size: 448). For each level, the correlation coefficients of the temperature and humidity were 0.66 and 0.57, respectively. Regardless of temperature and humidity, the correlation of each level was optimum at 500 hPa, followed by 700 and 850 hPa. Moreover, with respect to correlation, that for the temperature was more satisfactory than that for the dew point.

These results are attributable to the following reasons. The first is topography: mountains within 50 km from sounding stations were covered, and the highest-altitude mountain range was approximately 4 km tall. This meant that only the 500-hPa level was unaffected. The second is the configuration of the measuring equipment. Specifically, the sounding station furnished only single-point observations, and the weather balloon shifted horizontally with the wind, whereas AIRS furnished plane observations. Therefore, the horizontal resolutions of both methods were different. The third is differences in observation time. Specifically, most atmospheric conditions change gradually. However, an approaching weather system can cause a large and rapid change in the atmospheric temperature and dew point, which results in errors. Nonetheless, measurements of the average AIRS temperature and dew point around the stations were still representative of vertical atmospheric conditions around the station.

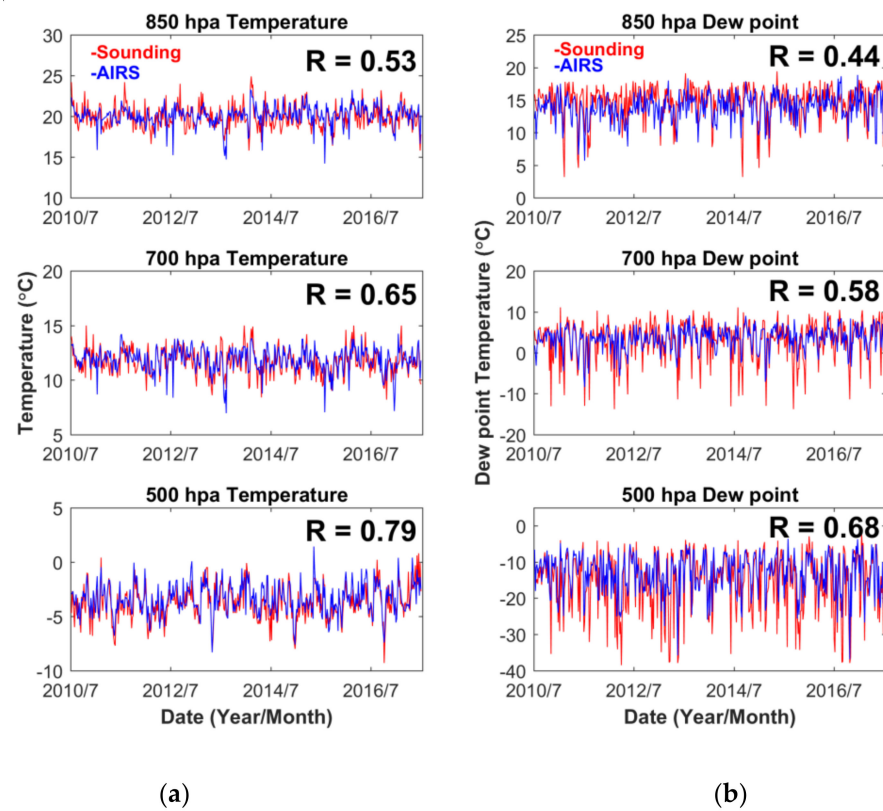


Figure 4. Comparison of AIRS (blue line) and radiosonde (red line) for (a) temperature, and (b) dew point for 850, 700, and 500 hPa (from top to bottom).

For radiosonde observations, the root-mean-square error (RMSE) and Standard deviation (SD) of the temperature and humidity, both before and after AIRS correction, are presented in Tables 4 and 5. In Table 4, temperature had the largest RMSE and SD at 850 hPa, followed by 700 hPa and 500 hPa. Subsequent to corrections through the equations in Table 2, the RMSE and SD of each level decreased, with 850 hPa having the highest correction margin, followed by 700 hPa and 500 hPa. This is attributable to the small error of the original level (500 hPa), resulting in a low correction margin. By contrast, the correction margin was larger at 850 hPa. Crucially, because of the lower RMSE and SD, the corrected AIRS temperature had a reduced dispersion that was closer to the radiosonde observation value, indicating that this study’s modified equation effectively made the AIRS temperature measurements closer to their radiosonde counterparts.

Table 4. RMSE and SD for 2017–2018 temperature measurements before and after correction.

Levels	500 hPa		700 hPa		850 hPa	
	Before	After	Before	After	Before	After
root-mean-square error	1.08	1.05	1.22	1.12	1.48	1.27
Standard deviation	1.11	0.94	1.18	0.83	1.31	0.79

Table 5. RMSE and SD for 2017–2018 dew point measurements before and after correction.

Levels	500 hPa		700 hPa		850 hPa	
	Before	After	Before	After	Before	After
root-mean-square error	4.93	4.92	4.16	4.13	3.79	2.73
Standard deviation	5.82	5.80	3.08	3.01	2.69	1.48

For dew point correction, the pre- and post-conditions were similar to those for temperature, and the RMSE and SD of each level were reduced. These results indicate that this study's modified equations effectively reduced errors for the AIRS measurements of temperature and humidity in Taiwan, thus making the AIRS measurements closer to their sounding-observation counterparts. In addition, as the altitude becomes higher, the RMSE and SD of the temperature and dew point observed by AIRS will increase. This result is similar to the previous studies [41,42].

3.2. Threshold for Afternoon Convection and Probability of Precipitation

This study investigated thermodynamically induced afternoon convection, which necessitated the use of the weak synoptic scale in the case selection. The METAR/SPECI showed cloud coverage at 0800–1200 LST was less than four oktas, which is defined as a weak synoptic scale. There must also be no significant weather systems, such as a weather front and typhoon, approaching the vicinity of the airports before and after convection.

The definition of rainfall in this study is METAR/SPECI afternoon precipitation data at 1200–1800 LST were checked to detect convection. The coverage area for detecting convection includes all surface stations within 20 km, and the airports were used as the center points. An indication of precipitation by at least one station was interpreted, as the occurrence of rain at the airport. By contrast, an absence of indication of precipitation by all stations was interpreted as the absence of rainfall at the airport.

The Taichung, Pingtung, Hualien, and Taitung airports marked by a red square in Figure 1 were selected as the research areas. In short, a forecast is correct if KI and TPW located at Q1 of Figure 3 and it rained in the afternoon. A forecast is also correct if KI and TPW located at Q2, Q3, or Q4 of Figure 3 and it did not rain in the afternoon. By contrast, a forecast is wrong if KI and TPW located at Q1 of Figure 3 and it did not rain in the afternoon. A forecast is also wrong if KI and TPW located at Q2, Q3, or Q4 of Figure 3 and it rained in the afternoon.

This study analyzed the afternoon convection thresholds of four different airports, because the threshold of convection occurrence changes depending on location [48]. Figure 5a,b map the distribution of KI and TPW for the Taitung and Taichung airports, respectively. The abscissa represents TPW, and the ordinate represents KI. The blue dots indicate those cases of afternoon convection, and the black dots indicate those cases where afternoon convection did not occur. Two red dotted lines represent the threshold values for the establishment of KI and TPW at the airports, and the thresholds were obtained from the highest forecast accuracy of the July and August of 2017–2018 data. The verification data in Figure 5 were for the July and August of 2019 and 2020.

As recorded in Figure 5a, the KI and TPW thresholds of Taitung airport's afternoon convection were 32.1 and 47.1, respectively. In 19 days, the predictions were located at Q1, and convection was predicted because $KI > K_h$ and $TPW > T_h$ (situated in Q1). However, 4 cases had no indications of precipitation at all stations within 20 km of Taitung airport, whereas 15 cases had afternoon convection. Therefore, the forecast accuracy of Q1 was 78.9% (15 hits over 19 cases). By contrast, 18 cases located in the Q2, Q3, and Q4 were forecasted to have no afternoon convection. Nonetheless, 4 of them had precipitation records at the stations within 20 km of the airport, whereas 14 cases had no precipitation

records. Therefore, the forecast accuracy of Q2 to Q4 was 77.8% (14 hits over 18 cases). Overall, 29 hits and 8 false alarms were identified among the 37 cases of Taitung airport. Therefore, the total forecast accuracy of Taitung airport was 29/37, or 78.4%.

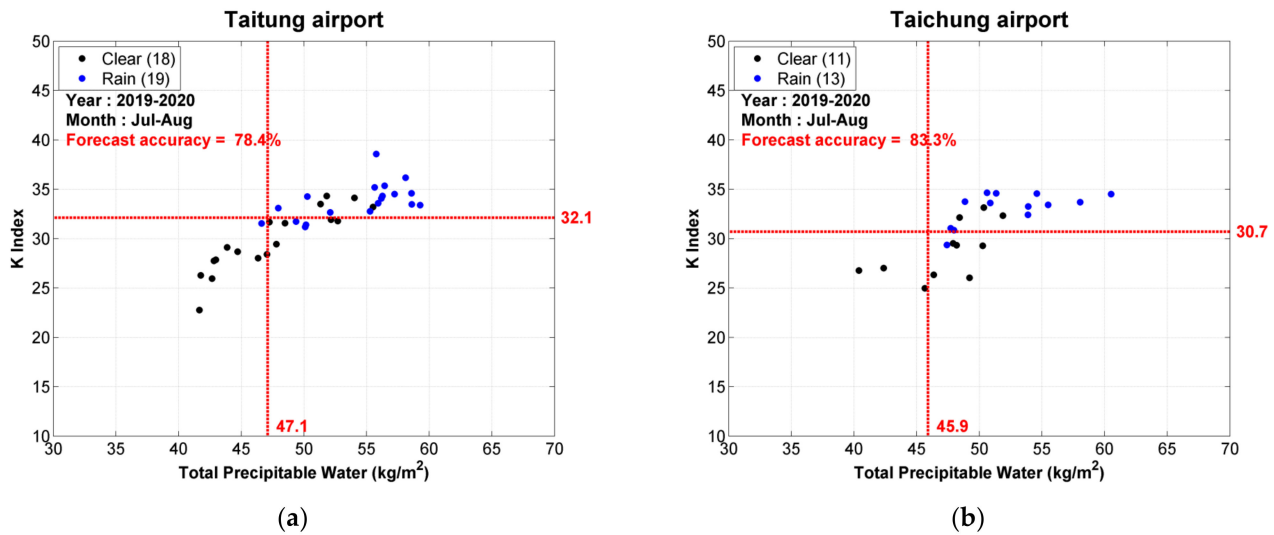


Figure 5. KI and TPW distribution map for (a) Taitung airport and (b) Taichung Airport. The blue and black dots are those cases with and without convection, respectively, and the red dotted lines indicate the thresholds for KI and TPW.

The same method for evaluating predictive accuracy was used for predictions for Taichung airport (Figure 5b). The forecast accuracy for afternoon convection in Q1 was 80% (12 hits over 15 cases), and the forecast accuracy for Q2, Q3, and Q4 was 88.8% (8 hits over 9 cases), for a total forecast accuracy of approximately 83.3% (20 hits over 24 cases).

All information such as the location of the four airports, the rainfall thresholds of KI and TPW for each airport, the accuracy of rainfall events (Q1 area), the accuracy of non-rainfall events (Q2–Q4 area), and the total accuracy are shown in Table 6. According to Table 6, the KI and TPW thresholds differ by region. This result indicates the stability index threshold of rainfall in different regions, which needs to be revised according to different locations.

Table 6. KI and TPW thresholds and forecast accuracy at the four airports.

Site Name	Location	Threshold of KI	Threshold of TPW	Forecast Accuracy of Q1	Forecast Accuracy of Q2–Q4	Total Accuracy
Hualien	23.98° N 121.6° E	27.7	44.3	82.1% (23/28)	80% (4/5)	81.8% (27/33)
Taitung	22.78° N 121.16° E	32.1	47.1	78.9% (15/19)	77.8% (14/18)	78.4% (29/37)
Pingtung	22.7° N 120.48° E	25.5	42.4	95.2% (20/21)	100% (0/0)	95.2% (20/21)
Taichung	24.26° N 120.62° E	30.7	45.9	80% (12/15)	88.8% (8/9)	83.3% (20/24)
All cases	-	-	-	84.3% (70/83)	81.3% (26/32)	83.5% (96/115)

The forecast accuracy and frequency of occurrence of afternoon convection in the four airports were further analyzed. The Taitung and Hualien airports (hereafter referred to as the eastern airports) are situated in more mountainous areas, as marked by the red square in Figure 1. By contrast, the Pingtung and Taichung airports (hereafter referred to as the western airports) were situated on almost flat terrain. As for the ratios of without

rainfall to rainfall with afternoon convection, those for the eastern and western airports were approximately 1:1.6 and 1:2.8, respectively. The eastern airports also had fewer rainy days than did the western airports. Moreover, the precipitation forecast accuracy and the total forecast accuracy for the western (~89%) airports were more favorable than those of the eastern airport (80%).

This difference in performance is attributable to the following reasons. First, because the eastern airports were situated in more mountainous areas, convection also depended on dynamic factors (and, to some extent, thermodynamic factors). Therefore, forecasting performance was worse for eastern airports because this study only considered thermodynamic factors. Second, atmospheric sounding was more accurate for western than eastern airports because western airports were not situated in mountainous areas. This result suggests the rainfall is related to terrain, elevation, slope, shape, and wind structure and so on [48–50].

This result suggests that precipitation products as well as the forecast precipitation indices that were derived from satellite data were susceptible to the influence of terrain. This is particularly true in Taiwan where mountainous areas account for 70% of the terrain. Therefore, such errors must be corrected prior to the use of satellite precipitation-related products. These results are similar to those of Yeh et al. (2019) [51].

The total forecast accuracy was lowest for Taitung airport (at 78.4%) because a mountain range dominated its landscape (within a 20-km radius) at a degree greater than that for other airports. There are a total of 115 cases for verification in this study. A total of 96 cases were forecasted correctly, and 19 cases were forecasted incorrectly. The total forecast accuracy rate was 84%. Furthermore, the accuracy rate of rainfall events is 84.3%, and the accuracy rate of non-rainfall events is 81.3%.

3.3. Case Studies

In addition to upgrading point information to area information for better applicability to airport personnel, the use of satellite data for the forecast of afternoon convection improves forecasting accuracy. The improvement percentage will be discussed in the next section. In this section, Hualien airport was used as an example. Two cases were analyzed to illustrate how AIRS measurements yield more accurate predictions than their radiosonde counterparts.

The first case occurred on 6 July 2018. The KI value was 31, as calculated from the radiosonde observation of the atmospheric sounding on the morning of that day; this KI value exceeded the threshold for afternoon convection (Table 6). An afternoon convection is forecasted to occur at the airport if the forecaster judges it to be so through the use of this set of radiosonde data. Figure 6a,b map the distribution of AIRS-derived KI and TPW. As illustrated in the figures, KI did not reach 20 and TPW did not reach 40 kg/m²; neither reached the threshold. Based on these data, the forecaster predicted no convection in the afternoon. No precipitation was recorded that afternoon at the observation stations within 20 km of the airport.

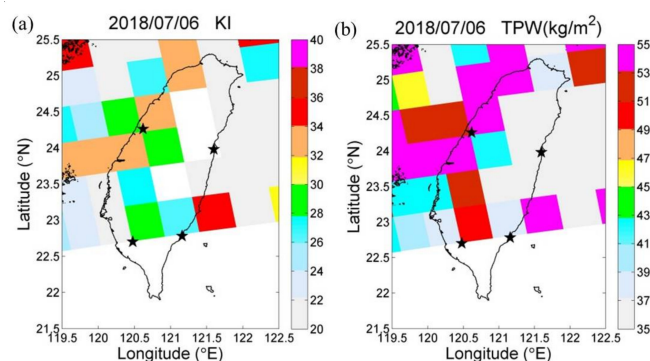


Figure 6. AIRS retrieval on 6 July 2018. (a) KI and (b) TPW distribution maps.

The second case occurred on August 9 of the same year. The radiosonde-derived KI was approximately 15, which did not reach the threshold. Figure 7a,b map the distribution of AIRS-derived KI and TPW. The KI near the airport was greater than 30, and the TPW was greater than 50 kg/m^2 , both of which exceeded the rainfall thresholds of Hualien airport. Thus, based on these radiosonde data, the forecasters predicted no convection at the airport. However, based on this study's satellite data, convection was forecasted at the airport. A rainfall event was determined to have occurred at the airport that afternoon.

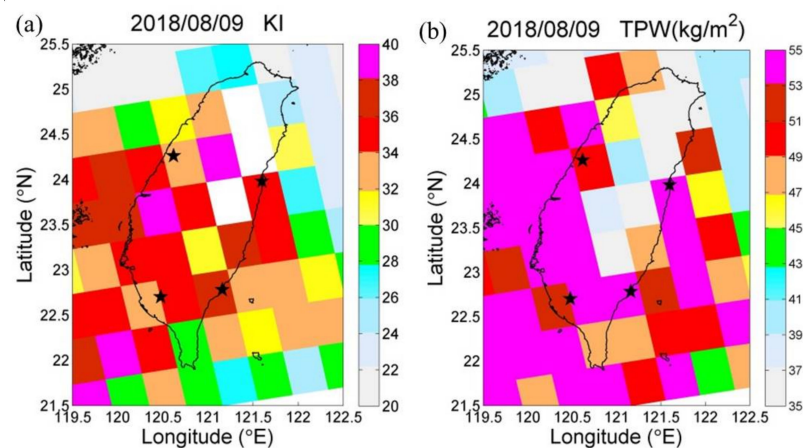


Figure 7. AIRS retrieval on 9 August 2018. (a) KI and (b) TPW distribution maps.

The aforementioned cases indicated that the atmosphere can change from stable to unstable (and vice versa) from the morning to the afternoon. Forecasters can reduce false weather forecasts if they use this study's satellite data instead of solely using radiosonde data. Because the atmospheric environment potentially changes every few hours, false forecasts are likely if changes in atmospheric stability are not accounted for. Moreover, because the time of the satellite scanning Taiwan is closer to the time when convection occurs in the afternoon, AIRS results in more effective forecasts of afternoon convection.

3.4. Improvement Percentage

In order to further determine the forecast accuracy of the method proposed in this study and see whether it is better than the traditional method, the results of this study were compared with those of radiosonde data, which are conventionally used by aeronautical meteorological forecasters, to compare the accuracy and practicability of both methods. In this study, only the radiosonde observations were used to forecast the afternoon convection at the airports in July and August of 2019 and 2020. The comparison was conducted only for Hualien airport because the available open-source radiosonde data covered only that airport.

Among the 33 cases that used radiosonde observations to forecast afternoon convection in Hualien airport, 24 cases were accurate and 9 cases were inaccurate, resulting in total forecast accuracy of 72.7%. By contrast, this study's total forecast accuracy of afternoon convection in Hualien airport using satellite data was, at 81.8%, higher, which was an improvement of 9.1%. Even if the forecast accuracy rate is improved compared with the previous method, the forecast accuracy rate still cannot reach 100%; this is the disadvantage of this research. In other words, there is still a possibility of incorrect forecasts using the forecasting method of this research, so it is still necessary to use manual assistance to observe weather changes to ensure flight safety. Another contribution of this study was its transformation of the original single-point sounding data into area data. This allows airports (such as the Taichung and Taitung airports) that have not launched weather balloons to use this study's method to forecast afternoon convection. Therefore, relative to the radiosonde method, this study's method is applicable to a wider range of airports.

4. Conclusions

This study uses satellite data to do airports nowcasting research. In other words, this study uses satellite data to predict the summer afternoon convection in the weak synoptic scale at Taiwan airports in Taichung, Pingtung, Hualien, and Taitung. Modified equations were established using 2010–2016 AIRS and radiosonde observation data, and 2017–2018 data were used to verify the accuracy of temperature and dew point of AIRS. The independent data (2019–2020) is used to verify the practicality and accuracy of this study's forecasting method. This study aimed to increase the number of airports that can be covered by the forecast by using the satellite's large swath. In addition, it also improves the accuracy of the forecast and the validity of the data, for the satellite scanning time is close to the time when convection occurs most frequently in Taiwan. The novel aspect of this research is to use satellite data closer to the time of convective rainfall than the radiosonde while considering two rainfall-related parameters to forecast afternoon convection. This study also takes into account that different airports have different environments, so different rainfall thresholds are established to improve the accuracy of rainfall forecasts.

AIRS atmospheric sounding products have good accuracy in the troposphere [35]. However, because of Taiwan's mountainous terrain as well as the difference between AIRS and radiosonde with respect to measurements of temperature and humidity, the deviation in low-troposphere measurements will differ depending on the season [31]. This resulted in an unsatisfactory correlation between temperature and humidity when AIRS measurements were directly compared with their radiosonde counterparts. Relevant factors must be considered, such as the FOV covering mountainous areas and various atmospheric conditions within 50 km of the radiosonde. After the numerical average, the correlation coefficients of temperature and humidity were increased by approximately 0.2 to 0.1.

For the temperature and dew point of the vertical altitude layer observed by AIRS and radiosonde, the correlation coefficient of 500 hPa is the best, because it is not affected by mountains. In addition, the temperature observed by AIRS is more accurate than the dew point. The reason is that the uncertainty of the dew point is greater than that of the temperature. Moreover, upon applying the modified equations established in this study, the RMSE and SD of temperature and humidity of each level were improved, thus demonstrating that the modified equations effectively reduce errors for AIRS measurements of temperature and humidity in Taiwan.

This study used AIRS data from 2017 and 2018 to obtain the airport afternoon convection threshold at Taichung, Pingtung, Hualien, and Taitung airports. Because the terrain around the western airports was relatively flat, the use of these thresholds to forecast the accuracy of afternoon convection was more favorable than that for the eastern airports. Using data from 2019–2020, the total forecast accuracy for the Taichung, Pingtung, Hualien, and Taitung airports was 83.3%, 95.2%, 81.8%, and 78.4%, respectively, with a total forecast accuracy of 84%. The main contribution of this research is to use scanning area to increase the available airports and improve the accuracy by 9.1% compared with traditional radiosonde forecasting methods. The improvement of forecast accuracy can reduce problems caused by inaccurate weather forecasts. These problems include flight safety issues, especially when aircraft take off and land; aircraft not being able to land at the scheduled airport, which affects the subsequent flight schedule; and the waste of fuel and increased costs entailed.

Author Contributions: Conceptualization, N.-C.Y.; methodology, N.-C.Y. and Y.-C.C.; data curation, H.-S.P. and C.-Y.C.; validation, N.-C.Y. and H.-S.P.; formal analysis, Y.-C.C. and C.-Y.C.; writing—original draft preparation, N.-C.Y.; writing—review and editing, Y.-C.C. and H.-S.P.; funding acquisition, Y.-C.C. and N.-C.Y. All authors have read and agreed to the published version of the manuscript.

Funding: This research was funded by Ministry of Science and Technology of Taiwan, grant number MOST 110-2111-M-344-001.

Institutional Review Board Statement: Not applicable.

Informed Consent Statement: Not applicable.

Data Availability Statement: The datasets of Aqua/AIRS and radiosonde used in this study are publicly available in the archives: https://disc.gsfc.nasa.gov/datasets/AIRS2RET_7.0/summary and <https://dbar.pccu.edu.tw/>, respectively (accessed on 1 October 2021).

Conflicts of Interest: The authors declare no conflict of interest.

References

1. Johnson, R.H.; Bresch, J.F. Diagnosed characteristics of Mei-Yu precipitation systems over Taiwan during the May–June 1987 TAMEX. *Mon. Weather Rev.* **1991**, *120*, 2540–2557. [CrossRef]
2. Lin, P.F.; Chang, P.L.; Jou, B.J.D.; Wilson, J.W.; Roberts, R.D. Warm season afternoon thunderstorm characteristics under weak synoptic-scale forcing over Taiwan Island. *Weather Forecast.* **2011**, *26*, 44–60. [CrossRef]
3. Wilson, J.W.; Mueller, C.K. Nowcasts of thunderstorm initiation and evolution. *Weather Forecast.* **1993**, *8*, 113–131. [CrossRef]
4. Chang, H.L.; Brown, B.G.; Chu, P.S.; Liou, Y.C.; Wang, W.H. Nowcast guidance of afternoon convection initiation for Taiwan. *Weather Forecast.* **2017**, *32*, 1801–1817. [CrossRef]
5. Wilson, J.W.; Schreiber, W.E. Initiation of convective storms by radar-observed boundary layer convergent lines. *Mon. Weather Rev.* **1986**, *114*, 2516–2536. [CrossRef]
6. Bohner, J. General climatic controls and topoclimatic variations in Central and High Asia. *Boreas* **2006**, *35*, 279–295. [CrossRef]
7. Ichiyanagi, K.; Yamanaka, M.D.; Muraji, Y.; Vaidya, B.K. Precipitation in Nepal between 1987 and 1996. *Int. J. Climatol.* **2007**, *27*, 1753–1762. [CrossRef]
8. Shrestha, D.; Sharma, S.; Hamal, K.; Jadoon, U.K.; Dawadi, B. Spatial Distribution of Extreme Precipitation Events and Its Trend in Nepal. *Environ. Sci.* **2021**, *9*, 58–66. [CrossRef]
9. Davis, R.E.; Stanmeyer, T.M.; Jones, G.V. A synoptic climatology of tornadoes in Virginia. *Phys. Geogr.* **1997**, *18*, 383–407. [CrossRef]
10. Kodama, K.; Barnes, G.M. Heavy rain events over the south-facing slopes of Hawaii: Attendant conditions. *Weather Forecast.* **1997**, *12*, 347–367. [CrossRef]
11. Derubertis, D. Recent trends in four common stability indices derived from U.S. radiosonde observations. *J. Clim.* **2006**, *19*, 309–323. [CrossRef]
12. Tu, C.C.; Chen, Y.L. Favorable conditions for the development of a heavy rainfall event over Oahu during the 2006 wet period. *Weather Forecast.* **2011**, *26*, 280–300. [CrossRef]
13. Seidel, D.J.; Sun, B.; Pettey, M.; Reale, A. Global radiosonde balloon drift statistics. *J. Geophys. Res.* **2011**, *116*, D07102. [CrossRef]
14. Li, J.; Liu, C.Y.; Zhang, P.; Schmit, T.J. Applications of full spatial resolution space-based advanced infrared soundings in the preconvective environment. *Weather Forecast.* **2012**, *27*, 515–524. [CrossRef]
15. Tobin, D.C.; Revercomb, H.E.; Knuteson, R.O.; Lesht, B.M.; Strow, L.L.; Hannon, S.E.; Feltz, W.F.; Moy, L.A.; Fetzer, E.J.; Cress, T.S. Atmospheric Radiation Measurement site atmospheric state best estimates for Atmospheric Infrared Sounder temperature and water vapor retrieval validation. *J. Geophys. Res.* **2006**, *111*, D09S14. [CrossRef]
16. Smith, W.L.; Revercomb, H.; Bingham, G.; Larar, A.; Huang, H.; Zhou, D.; Li, J.; Liu, X.; Kireev, S. Evolution, current capabilities, and future advance in satellite nadir viewing ultra-spectral IR sounding of the lower atmosphere. *Atmos. Chem. Phys.* **2009**, *9*, 5563–5574. [CrossRef]
17. Isioye, O.A.; Combrinck, L.; Botai, J.O. Retrieval and analysis of precipitable water vapour based on GNSS, AIRS, and reanalysis models over Nigeria. *Int. J. Remote Sens.* **2017**, *38*, 5710–5735. [CrossRef]
18. Jiang, J.; Zhou, T.; Zhang, W. Evaluation of Satellite and Reanalysis Precipitable Water Vapor Data Sets Against Radiosonde Observations in Central Asia. *Earth Space Sci.* **2019**, *6*, 1129–1148. [CrossRef]
19. Wang, X.; Jiang, H. A 13-year global climatology of tropical cyclone warm-core structures from AIRS data. *Mon. Weather Rev.* **2019**, *147*, 773–790. [CrossRef]
20. Tuller, S.E. The relationship between precipitable water vapor and surface humidity in New Zealand. *Mon. Weather Rev.* **1977**, *26*, 197–212. [CrossRef]
21. Liang, H.; Zhang, Y.; Cao, L.; Cao, Y. Temporal relations between precipitable water vapour and precipitation during wet seasons based on nearly two decades of data from the Lhasa River valley, Tibetan Plateau. *Int. J. Clim.* **2020**, *40*, 1656–1668. [CrossRef]
22. Makama, E.K.; Lim, H.S. Variability and Trend in Integrated Water Vapour from ERA-Interim and IGRA2 Observations over Peninsular Malaysia. *Atmosphere* **2020**, *11*, 1012. [CrossRef]
23. Kim, S.; Matyas, C.J.; Yan, G. Rainfall Symmetry Related to Moisture, Storm Intensity, and Vertical Wind Shear for Tropical Cyclones Landfalling over the U.S. Gulf Coastline. *Atmosphere* **2020**, *11*, 895. [CrossRef]
24. Taniguchi, K.; Minobe, Y. Impact of Global Warming on Extreme Heavy Rainfall in the Present Climate: Case Study of Heavy Rainfall in Kinugawa, Japan (2015). *Atmosphere* **2020**, *11*, 220. [CrossRef]
25. Parkinson, C.L. Aqua: An Earth-observing satellite mission to examine water and other climate variables. *IEEE Trans. Geosci. Remote Sens.* **2003**, *41*, 173–183. [CrossRef]

26. Aumann, H.H.; Chahine, M.T.; Gautier, C.; Goldberg, M.D.; Kalnay, E.; McMillin, L.M.; Revercomb, H.; Rosenkranz, P.W.; Smith, W.L.; Staelin, D.H.; et al. AIRS/AMSU/HSB on the Aqua mission: Design, science objectives, data products, and processing systems. *IEEE Trans. Geosci. Remote Sens.* **2003**, *41*, 253–264. [[CrossRef](#)]
27. Chahine, M.T.; Pagano, T.S.; Aumann, H.H.; Atlas, R.; Barnett, C.; Blaisdell, J.; Chen, L.; Divakarla, M.G.; Fetzer, E.J.; Goldberg, M.; et al. AIRS: Improving weather forecasting and providing new data on greenhouse gases. *Bull. Am. Meteor. Soc.* **2006**, *87*, 911–926. [[CrossRef](#)]
28. Li, J.; Huang, H.L.; Liu, C.Y.; Yang, P.; Schmit, T.J.; Wei, H.; Weisz, E.; Guan, L.; Menzel, W.P. Retrieval of cloud microphysical properties from MODIS and AIRS. *J. Appl. Meteorol.* **2005**, *44*, 1526–1543. [[CrossRef](#)]
29. Weisz, E.; Li, J.; Menzel, W.P.; Heidinger, A.; Kahn, B.H.; Liu, C.Y. Comparison of AIRS, MODIS, CloudSat and CALIPSO cloud top height retrievals. *Geophys. Res. Lett.* **2007**, *34*, L17811. [[CrossRef](#)]
30. Li, J.; Li, J.; Otkin, J.; Schmit, T.J.; Liu, C.Y. Warning information in a preconvective environment from the geostationary advanced infrared sounding system—A simulation study using the IHOP case. *J. Appl. Meteorol. Climatol.* **2011**, *50*, 776–783. [[CrossRef](#)]
31. Sedlar, J.; Tjernström, M. 2019: A process-based climatological evaluation of AIRS level 3 tropospheric thermodynamics over the high-latitude arctic. *J. Appl. Meteor. Climatol.* **2019**, *58*, 1867–1886. [[CrossRef](#)]
32. Liu, C.Y.; Li, J.; Weisz, E.; Schmit, T.J.; Huang, H.L. Synergic use of AIRS and MODIS radiance measurement for atmospheric profiling. *Geophys. Res. Lett.* **2008**, *35*, L21805. [[CrossRef](#)]
33. Liu, C.Y.; Liu, G.R.; Lin, T.H.; Liu, C.C.; Ren, H.; Young, C.C. Using surface stations to improve sounding retrievals from hyperspectral infrared instruments. *IEEE Trans. Geosci. Remote Sens.* **2014**, *52*, 6957–6963. [[CrossRef](#)]
34. Liu, C.Y.; Li, J.; Ho, S.P.; Liu, G.R.; Lin, T.H.; Young, C.C. Retrieval of atmospheric thermodynamic state from synergistic use of radio occultation and hyperspectral infrared radiances observations. *IEEE J. Sel. Top. Appl. Earth Obs. Remote Sens.* **2015**, *9*, 744–756. [[CrossRef](#)]
35. Divakarla, M.G.; Barnett, C.D.; Goldberg, M.D.; McMillin, L.M.; Maddy, E.; Wolf, W.; Zhou, L.; Liu, X. Validation of Atmospheric Infrared Sounder temperature and water vapor retrievals with matched radiosonde measurements and forecasts. *J. Geophys. Res.* **2006**, *111*, D09S15.
36. Ho, S.P.; Peng, L.; Vömel, H. Characterization of the long-term radiosonde temperature biases in the upper troposphere and lower stratosphere using COSMIC and Metop-A/GRAS data from 2006 to 2014. *Atmos. Chem. Phys.* **2017**, *17*, 4493–4511. [[CrossRef](#)]
37. Ross, R.J.; Elliott, W.P. Tropospheric Water Vapor Climatology and Trends over North America: 1973–93. *J. Clim.* **1996**, *9*, 3561–3574. [[CrossRef](#)]
38. Chen, B.; Liu, Z. Global water vapor variability and trend from the latest 36 year (1979 to 2014) data of ECMWF and NCEP reanalyses, radiosonde, GPS, and microwave satellite. *J. Geophys. Res. Atmos.* **2016**, *121*, 11442–11462. [[CrossRef](#)]
39. Zhao, J.; Li, T.; Shi, K.; Qiao, Z.; Xia, Z. Evaluation of ERA-5 Precipitable Water Vapor Data in Plateau Areas: A Case Study of the Northern Qinghai-Tibet Plateau. *Atmosphere* **2021**, *12*, 1367. [[CrossRef](#)]
40. Chen, W.J. The use of AVHRR data in TOVS retrievals. Ph.D. Thesis, National Central University, Zhongli, Taiwan, 1994.
41. Dirksen, R.J.; Sommer, M.; Immler, F.J.; Hurst, D.F.; Kivi, R.; Vömel, H. Reference quality upper-air measurements: GRUAN data processing for the Vaisala RS92 radiosonde. *Atmos. Meas. Tech.* **2014**, *7*, 4463–4490. [[CrossRef](#)]
42. Sun, B.; Reale, A.; Seidel, D.J.; Hunt, D.C. Comparing radiosonde and COSMIC atmospheric profile data to quantify differences among radiosonde types and the effects of imperfect collocation on comparison statistics. *J. Geophys. Res.* **2010**, *115*, D23104. [[CrossRef](#)]
43. Sun, B.; Reale, A.; Schroeder, S.; Seidel, D.J.; Ballish, B. Toward improved corrections for radiation-induced biases in radiosonde temperature observations. *J. Geophys. Res. Atmos.* **2013**, *118*, 4231–4243. [[CrossRef](#)]
44. Ingleby, B. *An Assessment of Different Radiosonde Types 2015/2016*; ECMWF Technical Memoranda: Reading, UK, 2017; p. 807.
45. George, J.J. *Weather Forecasting for Aeronautics*; Academic Press: Waltham, MA, USA, 1960.
46. Burpee, R.W. Peninsula-scale convergence in the south Florida sea breeze. *Mon. Weather Rev.* **1979**, *107*, 852–860. [[CrossRef](#)]
47. Li, J.E.; Liu, C.C.; Chao, C.C.; Yeh, N.C. A preliminary analysis in potential environment of convections in the summer by using satellite data. *Atmos. Sci.* **2005**, *33*, 189–214.
48. Shrestha, D.; Singh, P.; Nakamura, K. Spatiotemporal variation of rainfall over the central Himalayan region revealed by TRMM Precipitation Radar. *J. Geophys. Res. Atmos.* **2012**, *117*, D22106. [[CrossRef](#)]
49. Chen, Y.; Sharma, S.; Zhou, X.; Yang, K.; Li, X.; Niu, X.; Hu, X.; Khadka, N. Spatial performance of multiple reanalysis precipitation datasets on the southern slope of central Himalaya. *Atmos. Res.* **2021**, *250*, 105365. [[CrossRef](#)]
50. Sharma, S.; Khadka, N.; Nepal, B.; Ghimire, S.K.; Luintel, N.; Hamal, K. Elevation Dependency of Precipitation over Southern Slope of Central Himalaya. *Jalawaayu* **2021**, *1*, 1–14. [[CrossRef](#)]
51. Yeh, N.C.; Chuang, Y.C.; Peng, H.S.; Hsu, K.L. Bias adjustment of satellite precipitation estimation using ground-based observation: Mei-Yu front case studies in Taiwan. *Asia Pac. J. Atmos. Sci.* **2020**, *56*, 485–492. [[CrossRef](#)]